HHS Public Access

Author manuscript

Dev Biol. Author manuscript; available in PMC 2018 September 01.

Published in final edited form as:

Dev Biol. 2017 September 01; 429(1): 165–176. doi:10.1016/j.ydbio.2017.06.031.

Asymmetrically deployed actomyosin-based contractility generates a boundary between developing leg segments in *Drosophila*

Dan Ly, **Erin Resch**, **George Ordiway**, and **Stephen DiNardo**

Department of Cell and Developmental Biology, Perelman School of Medicine, the University of Pennsylvania, Philadelphia, PA 19104, United States

Abstract

The formation of complex tissues from simple epithelial sheets requires the regional subdivision of the developing tissue. This is initially accomplished by a sequence of gene regulatory hierarchies that set up distinct fates within adjacent territories, and rely on cross-regulatory interactions to do so. However, once adjacent territories are established, cells that confront one another across territorial boundaries must actively participate in maintaining separation from each other. Classically, it was assumed that adhesive differences would be a primary means of sorting cells to their respective territories. Yet it is becoming clear that no single, simple mechanism is at play. In the few instances studied, an emergent theme along developmental boundaries is the generation of asymmetry in cell mechanical properties. The repertoire of ways in which cells might establish and then put mechanical asymmetry to work is not fully appreciated since only a few boundaries have been molecularly studied. Here, we characterize once such boundary in the develop leg epithelium of *Drosophila*. The region of the pretarsus / tarsus is a known gene expression boundary that also exhibits a lineage restriction (Sakurai et al., 2007). We now show that the interface comprising this boundary is strikingly aligned compared to other cell interfaces across the disk. The boundary also exhibits an asymmetry for both Myosin II accumulation as well as one of its activators, Rho Kinase. Furthermore, the enrichment correlates with increased mechanical tension across that interface, and that tension is Rho Kinase-dependent. Lastly, interfering with actomyosin contractility, either by depletion of myosin heavy chain or expression of a phosphomimetic variant of regulatory light chain causes defects in alignment of the interfaces. These data suggest strongly that mechanical asymmetries are key in establishing and maintaining this developmental boundary.

1. Introduction

In patterning organs and tissues, a recurring principle is the subdivision of the cellular field comprising the tissue. Such subdivisions accomplish various tasks in organizing pattern. For example, cells in adjacent sectors often take on distinct fates, and / or restrict their progeny to one or the other subdivision. One of the earliest- and most well-defined subdivisions

Correspondence to: Stephen DiNardo.

Appendix A. Supporting information: Supplementary data associated with this article can be found in the online version at doi: 10.1016/j.ydbio.2017.06.031.

known is that of the anterior-posterior (AP) compartment subdivision of insect imaginal disks that acts as a unit of lineage-restriction (Garcia-Bellido et al., 1973; Morata and Lawrence, 1977). These compartments were also shown to be units of developmental identity, since Homeotic gene expression is regulated at the compartment level (Casanova et al., 1985). Vertebrate tissues also employ subdivision as a successful patterning strategy, since compartments have been documented in several cases, including at the midbrain-hindbrain boundary (Fraser et al., 1990; Zervas et al., 2004; Langenberg and Brand, 2005).

In addition to governing cell fate and lineage, the subdivision of a cellular field can be used to assign special signaling properties to one or the other territory, or to special cells flanking a boundary. The signaling cells can be sources for morphogens that aid in patterning the large cellular field. This has been described for the insect AP and other compartment boundaries (Nellen et al., 1996; Zecca et al., 1996; Micchelli and Blair, 1999; Rauskolb and Irvine, 1999), as well as in the vertebrate brain across rhombomeres or at the midbrain-hindbrain junction (McMahon et al., 1992; Crossley et al., 1996; Mellitzer et al., 1999; Xu et al., 1999; Calzolari et al., 2014).

Recently, it has been shown that the cells flanking such boundaries exhibit more than simply a unique pattern of gene expression. Boundary cells often exhibit differential cell mechanical properties compared with other cells in the tissue. These include adhesive and tensile networks that are used not only in shaping the boundary cells but in modulating their interactions with neighbor cells along the boundary. Thus, a main focus is investigating the underlying cellular properties of the common interface formed between cells flanking a boundary, and to understand how those properties implement the developmental program that lies behind the subdivision, whether that involves implementing a lineage restriction or inhibiting cell intrusions across a boundary due to intercalation events (for a review, see (Dahmann et al., 2011; Calzolari et al., 2014; Landsberg et al., 2009; Monier et al., 2010; Aliee et al., 2012; Umetsu et al., 2014)).

Cytoskeletal components that comprise actomyosin contractility networks are often enriched along boundary interfaces. This is the case at vertebrate rhombomere boundaries as well as the various boundaries studied in *Drosophila* embryos and imaginal disks (Calzolari et al., 2014; Landsberg et al., 2009; Monier et al., 2010; Aliee et al., 2012; Major and Irvine, 2005, 2006). Where tested, these interfaces exhibit relatively high tensile forces, but how those forces translate into the particular properties of the boundary are unclear. Furthermore, in some cases increased tension stabilizes and aligns cell interfaces, while in other cases it drives interface shrinkage (Landsberg et al., 2009; Monier et al., 2010; Aliee et al., 2012; Bertet et al., 2004; Zallen and Wieschaus, 2004; Blankenship et al., 2006; Bardet et al., 2013). Our understanding of how specific boundary properties arise necessitates the identification of more than the relatively few boundaries so far studied. The pretarsal / tarsal boundary of the developing *Drosophila* leg presents one such instance.

The adult Drosophila leg develops as an imaginal disk during larval stages. Incipient disk cells are specified late in embryogenesis, and invaginate. During larval stages, disk cells undergo extensive proliferation coupled to patterning by a well-characterized gene regulatory hierarchy acting along the antero-posterior, dorso-ventral and proximo-distal (PD)

axes. With regard to the PD axis, over-lapping subdivisions are initially established by upstream-acting ligands of the Wnt, BMP and EGF pathways, in part through the induction of the Distal-less gene (Lecuit and Cohen, 1997; Campbell, 2002; Galindo et al., 2002). Together, the three ligand-receptor signaling pathways generate concentric and slightly overlapping domains of gene expression along the proximo-distal axis during the third larval instar stage. Contributions from the Notch pathway and subsequent cross-regulatory interactions sharply define those domains during the mid- to late-third instar period (Rauskolb and Irvine, 1999; Kojima et al., 2000, 2005; Pueyo et al., 2000; Tsuji et al., 2000; de Celis Ibeas and Bray, 2003; Hao et al., 2003). Collectively, the concentric domains will eventually differentiate into the five tarsal segments of the leg and the pretarsus, located at the tip.

The boundary between the pretarsus and the fifth tarsal segment is particularly interesting as it is one of the two evolutionarily ancient subdomains of the arthropod limb (Snodgrass, 1935). In *Drosophila*, this distal region develops due to cross-regulatory interactions among a set of homeodomain- and LIM-domain-containing proteins, Aristaless (Al), C15 (also known as Clawless), the Bar family, and Lim1 and its cofactor Chip (Kojima et al., 2000; Tsuji et al., 2000; Pueyo and Couso, 2004; Campbell et al., 1993; Schneitz et al., 1993). This boundary constitutes a lineage-restriction, as late-induced clones can populate only one side of the pretarsal / tarsal boundary (Sakurai et al., 2007). Although there have been some morphological and genetic distinctions reported about cells on either side of the boundary, including differences in cell shape and the expression of certain cell surface molecules (Sakurai et al., 2007), the cell mechanics of this boundary have not been investigated.

Here we describe and quantify the striking alignment along the pretarsal / tarsal boundary compared to other cell interfaces across the disk. We also show that there are asymmetric enrichments for components of the actomyosin cytoskeleton. Finally, we test whether there is increased tension along this interface, and whether tension contributes to alignment.

2. Results

The boundary between the inner pretarsal domain and the adjacent tarsal domain is evident in the late third instar leg disk epithelium (Fig. 1). This boundary is located at the transition of low to high Clawless (C15) expression (Fig. 1A, inset; 1D). The interface was particularly prominent when cell profiles were revealed at the adherens junction level using phospho tyrosine epitopes (Fig. 1A, and inset; Fig. 1C). We will refer to the interfaces along this on-off gene expression boundary as “rails” (Fig. 1A inset, 1C). Analysis in later figures will also examine the properties along interfaces made from cells one column to the inside of the rail (Fig. 1C inset; −1 interface) or one column to the outside (+1 interface). Finally, we will refer to the cell interfaces orthogonal to the rail as “rungs” (Fig. 1C). Whereas pTyr was enriched along rails (Fig. 2A, B, B′), other factors, such as Bazooka / Par3, were enriched along rungs (Fig. 2A, C, C′). Quantitation confirmed the relative pTyr enrichment along rails (Fig. 2D, blue vs magenta; $p < 0.0001$, Mann-Whitney test; 4 disks, 203 and 274 interfaces), and the reciprocal enrichment of Baz/Par3 along rungs (Fig. 2D, purple vs green; $p < 0.0001$; 203 and 364 interfaces).

The tarsal / pretarsal boundary is dependent on *aristaless* (*al*) and *C15* function (Kojima et al., 2005; Campbell et al., 1993; Schneitz et al., 1993). As expected, depleting *C15* function by compartment-wide expression of a shRNAi directed against *al* or C15 significantly disrupted morphogenesis of the pretarsal region (data not shown and Suppl. Fig. 1). More incisively, reducing *C15* function by inducing small clones of cells caused irregularities in boundary alignment (Fig. 1E, bracket; C15 RNAi domains marked by co-expression of GFP in underlying nuclei). Depletion of *C15* also led to changes in Baz/Par3 enrichments. For instance, Baz/Par3 increased on rails when cells were depleted of *C15* (Fig. 1E″, between green arrows, and asterisk with arrowhead).

One striking quality of the pretarsal / tarsal boundary was the relative alignment observed along its common, pTyr-enriched rail interface (Fig. 1C; 2B). This suggested that a high degree of organization was imposed along this boundary. Normally, within epithelia, when tensile and adhesive forces are distributed evenly around cell perimeters, the epithelium exhibits hexagonal packing (Hayashi and Carthew, 2004). In these cases, angles between adjacent cell interfaces approach 120°. To contrast this relatively low-energy state with what was observed along the pretarsal / tarsal boundary, we quantified the angles that existed among the cell interfaces that comprised the rail (Fig. 3A, B). We found that the rail interfaces were strongly skewed toward 180° (Fig. 3C, blue dots; median angle = 171°, 4 disks, 120 interfaces). This contrasted to interfaces located far from the boundary (two or more cell diameters within the pretarsal region or within the tarsal region; Fig. 3A). Along those removed interfaces, the distribution of angles was more broad, and the median angle was reduced to 148° and 135°, respectively (Fig. 3C, magenta and green, 174 and 116 interfaces, respectively). Furthermore, the level of alignment along the rail significantly differed when compared to junctions within either the pretarsal or tarsal domain ($p < 0.0001$, Mann-Whitney test, for either comparison). Thus, cells making up the boundary exhibit a striking alignment, reflecting a higher energy state than that normally observed across the epithelium.

A well-studied, canonical developmental boundary is the Anteroposterior (AP) compartment border. While alignment along the leg AP boundary (Fig. 3, brown arrow) has not been reported, in other imaginal tissues the AP interface is more smooth than interfaces within either compartment (Landsberg et al., 2009; Umetsu et al., 2014). We found that the distribution of angles along the AP boundary of the leg epithelium was a bit broad, with the median alignment angle 156° (Fig. 3C). As expected from work in other imaginal tissues, the AP boundary was more aligned than interfaces within the pretarsal or the tarsal regions (Fig. 3C; compare brown to either magenta, 133°, $p < 0.0001$, or to green, 148°, $p = 0.007$). However, the leg disk pretarsal / tarsal rail was significantly more aligned than the leg AP boundary (Fig. 3C, $p < 0.001$, compare brown to blue dots; 4 disks, 120 versus 75 interfaces). Thus the pretarsal / tarsal rail boundary was more smooth than this well-studied developmental boundary.

Interestingly, closer inspection of the pretarsal / tarsal region revealed some alignment along interfaces directly adjacent to the boundary compared to those further inside either the pretarsal or the tarsal region. To confirm this observation, we measured the angles along interfaces made from cells one cell column to the inside of the rail (−1 interface) or one

column to the outside (+1 interface). Indeed, these −1 and +1 interfaces were significantly different from interfaces further away from the rail (Fig. 3C; $p < 0001$). The distribution of angles along the −1 interface was quite compact with a median of 169.5° (114 interfaces), suggesting it was quite similar to the rail (171°; $p = 0.015$). The angles comprising the +1 interface were a bit more spread, with a slightly lower median (160°, 126 interfaces, $p < 0.001$). Nevertheless, the data demonstrated a strong tendency towards alignment along interfaces directly adjacent to the rail. This suggests either that there exists an "alignment region" comprising more than just the pretarsal / tarsal boundary interface, or that there is some "spreading" of the morphogenetic effects occurring at the boundary.

2.1. Emergence of alignment during the third instar

Alignment emerged during the third instar, since early-stage disks did not exhibit the striking arcing alignment of cells (data not shown). This is as expected since the gene regulatory relationships that generate the pretarsal / tarsal developmental boundary occur from early-to-mid third instar (Campbell, 2002; Galindo et al., 2002; Kojima et al., 2000; Pueyo et al., 2000; Tsuji et al., 2000; Campbell et al., 1993). To address how alignment emerges, we attempted to use live-imaging to reveal the morphogenetic processes that created the aligned boundary. However, none of the culturing conditions that we tried with disks from early third instar were permissive to boundary development (see Section 4.3).

In lieu of real-time imaging, we analyzed development of the boundary using staged cohorts of larvae, which were then fixed and stained at different times before and at late third instar (Supplementary Fig 2). It was shown previously that the adhesion molecule Fasciclin II (FascII) becomes highly expressed on inner cells lining the arc (Sakurai et al., 2007; Kojima et al., 2000), and is asymmetrically distributed on membranes within those cells (Suppl. Fig. 2C, inset, red arrows). On those inner cells, Fasc II was enriched along rung interfaces, at an apical basal position just below the adherens junction where pTyr is enriched. Quantitation showed that Fasc II exhibited about 3-fold higher median levels compared to the adjacent rail interface (Fig. 4A; $p < 0.0001$; 3 disks, 122 rail, 130 rung interfaces). Thus we used Fasc II as a marker for emergence of the boundary.

By late L3, Fasc II was prominently and selectively enriched on rungs, when the rail was easily visualized (Suppl. Fig. 2C). Just twelve hours prior to this, however, Fasc II accumulated more diffusely, with some interfaces near the presumptive boundary apparent, but others less so (Suppl. Fig. 2B, compare arrow with area near asterisk). At eighteen hours prior to late third instar, Fasc II accumulation was quite low compared with just a few hours later (Suppl. Fig. 2A′, B″). Some suggestions of alignment were occasionally present (Suppl. Fig. 2A, compare arrow with asterisk), but their extent and stability could not be judged without the ability to image live.

Aside from the emergence of the pretarsal / tarsal boundary by late third instar, there was a previously noted cell size difference between pretarsal and tarsal cells (Kojima et al., 2000). For example, using phospho tyrosine epitopes to highlight cell profiles at the adherens junction level, the smaller profile of inner pretarsal cells was obvious compared to the larger profile tarsal cells (Figs. 1C, 2B). We found that this size differential also emerged during the mid to later third instar period (Suppl. Fig. 2) (Sakurai et al., 2007).

In several tissues the emergence of a boundary often reflects a developmental constraint, such as a lineage restriction. Indeed, late-induced clones are restricted, and can populate only one side of the pretarsal / tarsal boundary (Sakurai et al., 2007). We therefore focused next on mechanical properties that can constitute such a boundary.

2.2. Myosin II activity is involved in alignment

One likely candidate to drive the establishment of the boundary would be enhanced actomyosin contractility along prospective rail interfaces (Landsberg et al., 2009; Monier et al., 2010; Aliee et al., 2012). Indeed, the regulatory light chain (RLC) of Myosin II was selectively enriched along rails compared with rungs (Fig. 4B, compare blue and magenta dots; see also Fig. 6A, A″; $p < 0.0001$, Mann-Whitney test; 4 disks, 63 rail and 94 rung interfaces). F-actin was also enriched (data not shown). We also observed that an activator of Myosin II, Rho Kinase (RhoK)(Winter et al., 2001), was enriched along with Myosin II on rails relative to rungs (Fig. 4C; $p < 0.0001$, 3 disks, 77 rail and 109 rung interfaces).

These observations strongly suggested a role for Myo II in aligning the rail interfaces. To test this we examined disks depleted for *zipper* (*zip*), which encodes the heavy chain for Myosin II (Fig. 5). Indeed, the rail interfaces were more irregular in mutant compared with disks from sibling controls (Fig. 5A′ and B′). The median alignment angle in sibling controls 165° (134 interfaces over 4 disks) was significantly higher than that in mutant disks (151°; 294 interfaces, over 8 disks; Fig. 5C; $p < 0.0001$). Although the pretarsal / tarsal boundary was much more irregular, we did not observe significant numbers of C15 or Fasc II-labeled cells intruding into the tarsal region (Fig. 5B; see Section 3). Recall that interfaces flanking the rail (the −1 and +1 interfaces) normally are aligned more than interfaces more internal to the pretarsal / tarsal boundary. In *zip* mutants disks, we observed decreased alignment along the −1 interfaces (Fig. 5C, median angle 159° compared to 149°), though not the +1 interfaces.

The enrichment of RhoK strongly suggested polarized activation of Myo II along the rail interfaces. If this were the case, then disrupting the normal control of myosin activity might disrupt alignment. We tested this by expressing a phosphomimetic form of the Myosin Regulatory Light Chain, encoded by *spaghetti squash* (SqhDD). The expression of this phosphomimetic form generates defects in various tissues that rely on actomyosin contractility (Kasza et al., 2014; Vasquez et al., 2014; Mitonaka et al., 2007; Munjal et al., 2015). We restricted expression to the Engrailed subdomain of the developing leg disk, using En-GAL4, and marked those cells using UAS-GFP (Fig. 5D; see Section 4). This resulted in irregularities among boundary cells comparing control, anterior compartment cells, to posterior compartment cells expressing phosphomimetic Squash (Fig. 5D′, D″). Among control cells, alignment was relatively high along rails as expected (164°, 11 disks, 209 interfaces scored). In contrast, among cells expressing SqhDD, the alignment angles were broadly distributed with a median value significantly less than for controls (Fig. 5C; 145 °, $p < 0.0001$, Mann-Whitney test, 11 disks, 197 interfaces). The expression of SqhDD also compromised alignment along the −1 and +1 interfaces as well (Fig. 5C). These data suggest that interfering with regulated MyoII activity can interfere with alignment (see Section 3).

2.3. Cell interfaces along the boundary are under tension

With Myosin II implicated in alignment, its enrichment along the rail suggested polarized activity that might lead to increased tension along rail compared with rung interfaces. Relative tension can be inferred by quantifying the initial retraction velocity observed of adjacent cell vertices after scission of the cortical cytoskeleton along an interface (Farhadifar et al., 2007; Fernandez-Gonzalez et al., 2009). Indeed, we found that the peak retraction velocity was several-fold higher along rails compared to rungs (Fig. 6C, D; $p < 0.0001$, 14 and 13 interfaces, respectively). We also observed a significant difference in the maximum displacement of the retracted vertices, comparing rail to rung (Supplementary Fig 3; $p < 0.0001$). Furthermore, the tension along rails was sensitive to inhibition by either of two Rho Kinase inhibitors (Fig. 6C, D; $p < 0.0001$, 14 and 10 interfaces; see Section 4). In fact, in the presence of Rho Kinase inhibitor, the peak retraction velocity along rails was reduced to that of the rungs in the absence of inhibitor (Fig. 6C, D; $p = 0.9$; 13 and 10 interfaces). Maximum displacement was also reduced to that for the rungs (Supplementary Fig 3). We confirmed that the reduction of tension along rails in the presence of inhibitor correlated with a significant depletion of RLC-mCherry from rails (Fig. 4B, compare blue and green dots; 6B″; $p < 0.0004$, 63 and 48 interfaces). Collectively, these data suggest that actomyosin contractility is involved in maintaining tension along the aligned rail interfaces.

Finally, we also tested whether the interfaces directly adjacent to the rail were under tension, since these were partially aligned. We cut interfaces along the −1 interface or the +1 interface. Both flanking interfaces exhibited lower peak retraction velocities than the rail (Fig. 6D; $p < 0.003$ for each comparison to the rail; 17, 16 and 15 interfaces, respectively). Flanking interfaces exhibited lower maximum displacement values also (Supplementary Fig 3). Even though the neighboring interfaces were less tensed than the rail, we did observe slightly higher tension along flanking interfaces compared to the rungs (Fig. 6D). There was a slightly higher median value (roughly 0.14 versus 0.05 μm/s) but also more of a spread in tension values. This suggests that there exists some tension along the flanking interfaces, in agreement with the partial alignment we observed (Fig. 3C).

2.4. Alignment is sensitive to Rho Kinase inhibition

If increased tension was important to alignment, then release of that tension might cause alignment defects. Therefore, we monitored alignment as disks were cultured before and after addition of the Rho Kinase inhibitor. Initially, cultured disks exhibited alignment of the rail as well as flanking interfaces, as expected. For example, at the first time point taken in culture, the rail was aligned (Fig. 7A, blue arrow, inset). Additionally, inspection showed that the aligned cells tended to be rectilinear in shape as noted previously (Sakurai et al., 2007). Upon addition of the Rho Kinase inhibitor, alignment became compromised and the cells became more trapezoidal (Fig. 7B). We quantified the change in alignment by measuring the angle along the rail before and after addition of inhibitor. Before addition of inhibitor rail angles exhibited a fairly tight distribution, with a median close to 170°, as expected (Fig. 7D, rail, blue dots). Thirty minutes after addition of the inhibitor, the distribution had spread significantly, and the median angle shifted to less than 150° (Fig. 7D, rail Inh, blue dots; $p < 0.0001$, Mann-Whitney test, 3 disks, $n = 77$ and 75 interfaces). This suggests strongly that a Rho Kinase inhibitor-sensitive step was necessary to maintain

alignment. Together with the observed depletion of Myosin II after inhibitor treatment (Figs. 4B, 6B), these data suggest that actomyosin contractility was important in maintaining the pretarsal / tarsal boundary.

The inhibition of Rho Kinase had effects on the interfaces flanking the rail. For instance, before addition of the inhibitor the −1 interface (Fig. 7A, magenta in inset) was relatively aligned, exhibiting a median angle of 164° (Fig. 7D, magenta dots). The +1 interface also appeared aligned, with a median approaching 159°, but exhibited more of a spread of angles (Fig. 7D, green dots). Addition of the Rho Kinase inhibitor decreased alignment along both of these flanking interfaces. For the −1 interface, median alignment decreased from 164° to 137° ($p < 0.0001$; n = 79 and 78 interfaces), while the +1 interface exhibited a similar magnitude in decreased alignment (159° to 139°, $p < 0.0001$, n = 76, 77). The change in alignment among flanking cells could be a direct consequence of Rho Kinase inhibitor acting locally on each flanking interface, or be driven by the altered alignment at the pretarsal / tarsal interface itself (see Section 3.1).

2.5. Alignment can be induced rapidly

It was frustrating that we could not image the development of the aligned interface live. However, the breakdown in alignment upon Rho Kinase inhibitor treatment suggested a way to visualize initial formation of the aligned boundary, if alignment could be restored after washout of the inhibitor. Indeed, thirty minutes after removal of inhibitor, rail angles returned to a fairly tight distribution, with a median close to 170° exhibiting no significant difference from that observed before inhibitor treatment (Fig. 7C, blue arrow in inset; 7D, rail Recovery, $p = 0.141$, n = 77 and 74 interfaces). A similar return to alignment was observed for the −1 interface (Fig. 7C, magenta arrow in inset). Note that after recovery, both the distribution and median angles for inner column of cells were not significantly different than that before inhibitor treatment ($p = 0.662$, n = 79, 64). The +1 interface behaved somewhat differently, as it did not recover alignment fully. Its median angle decreased from 159° to 139° upon inhibitor treatment, but only recovered to 144° after inhibitor withdrawal ($p = 0.073$, n = 77, 77). Nevertheless, these data demonstrated that rail alignment was significantly reversible, and could be re-established rapidly.

We wished also to test whether tension was re-established upon inhibitor withdrawal. Therefore we cultured disks without inhibitor, and carried out a small number of rail cuts to verify the baseline peak retraction velocity prior to inhibitor treatment. Rho Kinase inhibitor was then added, which reduced the median peak retraction velocity as expected (1.4 compared to 0.3 μm/s, $p = 0.028$, n = 3 and 4 cut interfaces). We next washed out the inhibitor, and performed a set of cuts beginning fifteen minutes after washout. As a consequence, the median peak retraction velocity increased more than two and a half fold (0.3–0.8 μm/s, $p = 0.0028$, n = 4 and 9 interfaces). These data suggest that mechanical properties of the pretarsal / tarsal boundary begin to be re-established quickly upon re-engagement of the actomyosin contractile network.

3. Discussion

A key component comprising a developmental boundary is the special mechanical properties imposed to its interfaces. Insights into these properties have been gained from the few tissues that have been studied, such as rhombomere boundaries in the vertebrate (Mellitzer et al., 1999; Xu et al., 1999; Calzolari et al., 2014), but especially the study of several boundaries in *Drosophila* (Landsberg et al., 2009; Monier et al., 2010; Aliee et al., 2012; Röper, 2013). The latter studies in Drosophila have afforded much higher resolution so far than study of rhombomeres. Still, relatively few boundaries overall have been studied, and that makes it difficult to draw any generalizations for how the underlying mechanics makes the boundary. Here we report our initial studies on the late-arising developmental boundary necessary for leg segmentation. The pretarsal / tarsal boundary was more aligned than the canonical AP compartment boundary. The rail exhibits an asymmetry in actomyosin accumulation as well as one of its activators, Rho Kinase. We showed that this results in increased tension along the boundary, which is important in aligning its interfaces.

3.1. Polarized actomyosin enrichment and its disparate outcomes

We show here that polarized actomyosin enrichment leads to increased cell bond tension along the pretarsal / tarsal interfaces. The fold increase of tension compared with the orthogonal rung interfaces is in line with differences observed in several other tissues, such as the Antero-posterior and dorso-ventral compartment boundaries (Landsberg et al., 2009; Aliee et al., 2012; Röper, 2013). Here, along the pretarsal / tarsal interface, actomyosin contractility generates a very smooth, arcing boundary. The alignment is significant, as it is even more aligned than the well-studied AP compartment boundary. In itself, this fact strongly suggests that study of the pretarsal / tarsal boundary will complement the information obtained though study of other developmental boundaries.

Our data revealing enrichment of the Myosin II regulatory light chain as well as Rho Kinase along rail interfaces strongly implicates contractility in alignment, and the degree of mis-alignment observed in zip mutants supports this contention (Fig. 5B, C). Furthermore, treatment with a Rho Kinase inhibitor reduced actomyosin enrichment and released tension along the rail, rapidly generating a less aligned state (Fig. 7). In addition, since removal of the Rho Kinase inhibitor led to the rapid re-establishment of alignment (Fig. 7), the data collectively argue that asymmetric contractility can drive this alignment event. Still, Rho Kinase inhibitors can affect other protein kinases (Atwood and Prehoda, 2009), such as Atypical Protein Kinase (aPKC). Thus, even though we used a quite selective Rho Kinase inhibitor, it is still possible that another kinase also contributes to alignment, perhaps targeting a factor in addition to the myosin regulatory light chain.

The expression of a phosphomimetic form of the Myosin II regulatory light chain generated defects along the rail. The precise mechanism involved awaits live-imaging the formation of the aligned interface. Without that capability in this epithelium, we cannot determine whether the phosphomimetic form of the Myosin II generated defects due to decreased cycling between on and off states along interfaces normally enriched for myosin, or to increased activity along the normally depleted (rung) interfaces (Kasza et al., 2014; Vasquez

et al., 2014; Mitonaka et al., 2007; Munjal et al., 2015). Nevertheless, regulated contractility is certainly important to alignment.

Actomyosin enrichment and the resultant increased tension is a theme observed repeatedly along cell interfaces. Interestingly, the outcome of that increase in tension can be quite different in different circumstances. In some cases, tension stabilizes cell interfaces, as has been observed along the parasegment boundary of the embryonic epithelium, as well as the AP and DV compartment boundaries in developing imaginal disk epithelia (Landsberg et al., 2009; Monier et al., 2010; Aliee et al., 2012). While actomyosin enrichment leads to stabilization in those cases, in other instances, enrichment and the associated increased tension drives interface shrinkage. Those shrinkage outcomes are crucial to the directed junctional remodeling events necessary for convergence extension (Bertet et al., 2004; Blankenship et al., 2006). Similar shrinkage events are also observed in tissues at steady-state. For example, across the epithelial field in the developing wing, junctional shrinkage events maintain the proper geometry of cell packing (Bardet et al., 2013). Just how actomoysin enrichment and junctional tension can be directed toward two quite diametrically opposed outcomes, shrinkage or stabilization, is unclear at present. This issue will only be resolved by examining more boundaries of each class, and by identifying more components that act along those interfaces.

In fact the pretarsal / tarsal boundary described here has several features in common with another interface described previously in our lab. In the late embryonic epidermis, well-after convergence and extension, a select set of cells within each parasegment organizes into aligned columns (Walters et al., 2006; Price et al., 2006; Simone and DiNardo, 2010). We have found that those aligning cell columns exhibit enrichments similar to those described here along the smooth, arcing pretarsal / tarsal rail. In addition, in both cases the cells that constitute the boundary assume elongate, rectilinear shapes (Sakurai et al., 2007; Walters et al., 2006; Simone and DiNardo, 2010). A comparison of the mechanics underlying these two alignment events could potentially reveal how actomoysin enrichment and junctional tension can be directed toward stabilization.

Besides exhibiting alignment, some boundary interfaces, such as the AP and DV compartment boundaries, are resilient to challenges from neighboring cells, whether from cell division or intercalation. The mechanical basis for this is becoming more clear (Landsberg et al., 2009; Monier et al., 2010; Aliee et al., 2012). The pretarsal / tarsal boundary develops a late-acting lineage-restriction (Sakurai et al., 2007), so it is interesting to consider the degree to which increased tension contributes to the restriction. Interestingly, in depleting or manipulating Myosin II activity the pretarsal/tarsal boundary became very irregular (Fig. 5). Yet, we did not find evidence for “invasions” from one territory to the other, at least not in these fixed preparations. This suggests that tension is not sufficient for this restriction in the leg. Perhaps like the DV compartment in the wing a combination of mechanical tension, as seen here, plus oriented divisions and cell elongation contribute to boundary integrity (Aliee et al., 2012). Alternatively, the affinity properties of the pretarsal versus tarsal cells may well contribute to the lineage restriction (Sakurai et al., 2007).

Finally, we note that the interfaces flanking the rail are also aligned to a significant degree. This differs from the situation observed along the AP compartment boundary where the adjacent interfaces were used as examples of relatively unaligned interfaces (Aliee et al., 2012). That raises the interesting question of whether the interfaces flanking the rail are actively aligned. For instance, machinery similar to that deployed along the rail might align the −1 and + 1 interfaces. Alternatively, the flanking interfaces might be aligned only passively, as a consequence of the geometry enforced by the rail interface on the other cell interfaces. If there is an active process aligning the flanking interfaces, MyoII would appear to be minimally involved. We observed no significant enrichment of MyoII along the −1 interface compared to the adjacent rung (Fig. 4, light blue and light magenta dots), and although these interfaces retained some tension, the level was much reduced along the −1 and + 1 interfaces compared to the rails (Fig. 6D).

3.2. Establishment of the boundary

We do not know yet how the polarized enrichments are first established along the pretarsal / tarsal boundary. There is a fairly well-understood gene regulatory hierarchy that establishes the pretarsal and tarsal territories during the mid third instar period of development (Campbell, 2002; Galindo et al., 2002; Kojima et al., 2000; Pueyo et al., 2000; Tsuji et al., 2000; Campbell et al., 1993). The initially rough borders between the two territories are subsequently refined by further cross-regulatory interactions. Thus, it is no surprise that interfering with the transcriptional regulator, *C15*, can cause defects along the boundary (Kojima et al., 2000, 2005) (Fig. 1E′, E″; Supplementary Fig 1). In addition, among the factors that are genetically regulated by this transcriptional circuitry are Fasciclin II and the leucine rich proteins, Capricious and Tartan (Caps; Trn) (Sakurai et al., 2007). However, it is not known how direct that regulation might be. Moreover, neither removing Fasciclin II, nor both Caps and Trn, generated phenotypes that seemed clarifying (Sakurai et al., 2007). This suggests that key factors remain to be defined. A similar limitation extends to the parasegmental, AP and DV boundaries. While the Wingless, Hedgehog and Notch pathways, respectively, have been implicated at those boundaries (Monier et al., 2010; Rudolf et al., 2015; Michel et al., 2016), the analyses still leave open the possibility that control by each of those pathways is indirect. Unraveling the direct links from cell signaling to the mechanics of tissue boundaries remains an important goal in studying morphogenesis.

4. Materials and methods

4.1. Fly stocks

Larvae were grown in uncrowded vials, at 25°C unless indicated, and w^{1118} was used as wild type. The following transgenic lines were also: UAS-Clawless RNAi (TRiP, FBst0027649 – used for Fig. 1 and Supplemental Fig. 1; FBti0128922; FBst0035018); UAS-Aristaless RNAi (FBst0026747); En-GAL4 recombined with UAS-GFP (FBti0002970, FBrf0152364); Hh-GAL4 (FBti0017278; (Tanimoto et al., 2000)); Tub-GAL80ts (FBti0027797); UAS-Sqh. DD, (FBal0263515; Mitonaka, 2007]); UAS-Sqh. EE::FLAG (FBal0243601; (Bertet et al., 2009); P{AyGAL4}25 P{UAS-EGFP}5a2 (FBst0064231). Live imaging was conducted on stocks carrying Ubi-DE-cad-GFP (FBtp0014096) (Oda and

Tsukita, 2001) and sqh-mCherry (A11) (FBtp0065864) (Martin et al., 2009); or RhoK{K116A}.GFP (FBal0296492) (Simões et al., 2014).

To deplete *C15* or *aristaless* in small groups of cells, clones expressing the RNAi transgene were induced in progeny of the cross: HS-FLP; RNAi × P{AyGAL4}25 P{UAS-EGFP}5a2. Vials containing 4 -to 5-day-old larvae were subjected to a 30 min, 37° heat shock, and larvae at late L3 were selected for dissection, fixation and staining. We discriminated late, crawling L3 larvae from earlier L3 stages by using food containing blue dye (Maroni and Stamey, 1983), and harvesting those with a cleared gut as late L3. For Supplementary Fig 2 we used vials containing blue food dye, and allowed young adult flies to lay eggs for 5 h, to seed the vials at low density. Vials were maintained at 25 °C and larvae picked at appropriate stages. Panel “C” shows a representative late L3 defined by a gut cleared of blue food dye. Under our culture conditions these larvae averaged just over 120 h old. The earlier panels present disks from larvae harvested either 12 h (panel B) or 18 h (panel A) prior to those late L3 stage larvae.

Mis-expression or knockdown used $GAL80^{ts}$ for temporal control. En-GAL4 UAS-GFP; Tub-$GAL80^{ts}$ was crossed to either UAS-Sqh. DD or UAS-C15 RNAi at 18°, and either maintained at permissive temperature for GAL80 (as one of the controls), or upshifted to 29° at the late L2 or early-to-mid L3 stage. For experiments expressing Sqh. DD, the results section compared values from anterior and posterior compartment cells in disks carrying En-GAL4 > Sqh. DD. The relative alignment of these anterior compartment cells did not differ compared to alignment for anterior or posterior compartment cells among disks not carrying En-GAL4. Appropriate crosses also generated larvae carrying Hh-GAL4 > Sqh. EE::FLAG Anti-FLAG stains consistently showed high-level expression of Sqh. EE in all posterior compartment cells; expression was too high to assign values to specific interfaces. Thus, this condition likely led to mis-regulation of MyoII activity along all interfaces. We also used anti-Zipper to test whether expression of the Sqh. EE might alter the normally-observed enrichment for Myo II along rail interfaces. However, the quality of the anti-Zipper stain was too variable for analysis in this epithelia.

4.2. Immunofluorescence

Appropriately staged larvae were crudely dissected in Drosophila Ringers buffer, and fixed in 4% formaldehyde, PBS, 0.1% TritonX-100 (PTx) for 20 min. Carcasses were washed with Ptx and then blocked for one hour in PTx containing 4% normal donkey serum. Samples were incubated overnight at 4 °C with the appropriate primary antibody mix diluted in block: Chicken anti-GFP (1:2000, Aves GF-1020), Rat Anti-C15 (1:1000, gift from G Campbell), Rat anti-E-Cadherin (1:20, DSHB), mouse anti Fasc II (DSHB), Rabbit Anti-Bazooka (1:1000, gift of A. Wodarz, GST N-term (Wodarz et al., 1999)), Mouse anti-phospho tyrosine 4G10 (1:1000, Millipore); rabbit anti-Zipper (1:1000, gift of Dan Kiehart); mouse anti-FLAG (1:5000, Sigma F3165). Secondary antibodies were labeled with Alexa488, Cy3, Cy5 or Alexa 690.

Images were acquired on a Zeiss Imager with Apotome using a 40×, 1.2 NA lens, or using a Leica confocal system with Yokogawa CSU-X1 spinning disk, using either a water

immersion 40×, (NA. 1.1) or 63 (1.2), or an oil imersion 100× (1.3) lens, driven by Metamorph (v7.8.4).

4.3. Live time-lapse imaging

Appropriately staged larvae were crudely dissected in Ringers solution and placed adjacent to the imaging cover slip inside a MatTek imaging dish, with fresh Ringers. Disks were separated from the carcass using fine tungsten needles, and each disk was floated over the cover slip and directed to settle, peripodial side down, onto the poly-lysine-coated coverslip. The Ringers buffer was removed and replaced gently with imaging media: Schneider's insect media (GIBCO 21720-024), 15% FBS (GIBCO 26140-111), 0.5× penicillin/ streptomycin (Invitrogen, 15140-122) and 0.2 mg/ml insulin (Sigma SLBD6620). For inhibitor treatments, after imaging sufficiently to establish a pretreatment standard, media was carefully aspirated and quickly but gently replaced with fresh media containing the diluted Rho Kinase inhibitor. To test recovery-from-inhibitor, after imaging in the presence of inhibitor the media was gently exchanged three times to wash out residual inhibitor, and finally replaced with fresh media for further imaging. New cuts were begun about ten to fifteen minutes after the washout, and took place over the next approximately 35 min (Fig. 7). In preliminary work we used the Rho Kinase inhibitor Y-27632 (Sigma, Y0503) at 380 μM. All the data reported here made use of the more potent and selective Rho Kinase inhibitor, H-1152, at 10 μM (Santa Cruz, sc-203592; K_i = 1.6 nM for Rho Kinase compared with K_i = 140 nM of Y-27632). Disks were imaged on either a Leica DM16000 B inverted spinning disk confocal or an Olympus IX71 inverted spinning disk confocal for up to ~3 h. Time lapses, with intervals of 5–20 min depending on the experiment, were acquired using water immersion lenses: either 40× / 1.1 NA, or 63×/1.20.

In the process of carrying out initial experiments using either Rho Kinase inhibitor, we discovered that the inhibitor loses potency over time. Frequently, over the first 60 min of treatment with inhibitor, we observed the phenotypes reported here. However, by about 90 min in the presence of inhibitor, the effects had worn off (e.g., interfaces appeared to re-align). In fact, recognizing those reversals led us to realize that we could attempt a more acute “wash-out” and recovery test reported here. The loss of potency could be caused by efflux of the inhibitor or by its metabolism, and the extent of such effects might be different for other inhibitors.

In attempts to observe the morphogenesis along the pretarsal / tarsal boundary, we tried several live-imaging protocols, culturing leg disks from late L2 or early L3 stages (Farhadifar et al., 2007; Currie et al., 1988; Aldaz et al., 2010; Zartman et al., 2013). Some attempts included fly or larval extracts, and / or 20-hydroxyecdysone. In our hands, none of these attempts allowed development of the boundary, even though mitotic divisions continued.

4.4. For laser ablation and quantifying retraction velocity

Typically, a two-channel z-stack was first acquired for each leg disk, or each region, prior to interface ablation. To limit any effect of global relaxation, cuts were limited generally to two per quadrant for each leg disk. The ablating beam generated by a MicroPoint laser

emanating from a 405 nm dye cell, was focused to the rail or rung interface through a 100×, 1.3NA lens, using Andor IQ3.2 software. The micro-point laser settings were optimized prior to each session to the minimal power required for junction severing. Simultaneously, Metamorph software was set up to stream single color images from the plane of the adherens junction (ECad-GFP) where each exposure was 250 ms. Acquisition was begun, and then the laser fired to ablate that interface selectively. Post-ablation acquisition would continue for 1–3 min.

After acquisition, the ablated interface was identified, and the time stack cropped, with the ablated interface oriented vertically, and a montage created that consisted of one pre-ablation frame, followed by 60 s worth of post-ablation frames, each at 5 s intervals; analyses carried out at 1 s intervals generated the same results. The X-Y coordinates for the vertices above and below the cut interface were mapped in Image J, exported to a spreadsheet. Peak retraction velocities were determined from displacement over time, and are presented in the scatter plots. Maximum displacement was also extracted and plotted in Supplemental Fig. 3.

4.5. Quantification of alignment and fluorescence intensities

For display as well as for quantification, after background subtraction, maximum projections were made from 2 to 3 slices encompassing the adherens junction level of the epithelial cells in question. In the case of Fasc II accumulation, the slices were centered just basally to the adherens junction. Interface angles were measured using the angles tool in Image J. Data was compiled in a spreadsheet, imported into GraphPad Prism 7 for statistical analysis (Mann-Whitney non-parametric tests) and assembling scatter plots. For measuring affects on alignment before, during an after recovery from Rho Kinase inhibitor treatment, live-imaging was carried out using 5 min intervals.

To analyze cell profiles for Supplementary Fig 1, we segmented the cell outlines using SeedWaterSegmenter (Mashburn et al., 2012), and imported the resulting thresholded cell outline image into PackingAnalyzer (Farhadifar et al., 2007) to return area parameters for pretarsal or tarsal subsets of cells.

To quantify fluorescent intensities, images were acquired at the identical exposure and gain. A subset of the z slices that would be analyzed were background subtracted, and then projected using the Max intensity setting in Image J. The file was imported into Siesta (Fernandez-Gonzalez and Zallen, 2011), and interfaces were highlighted manually, and their intensity values exported and analyzed in Prism 7.

Supplementary Material

Refer to Web version on PubMed Central for supplementary material.

Acknowledgments

We especially thank Katy Ong for key conceptual discussions, as well as expert advice on laser ablation and its analysis. We thank G. Campbell, A. Wodarz, Dan Kiehart, A. Martin, J. Zallen, Y. Nishida, T. Mizuno, K. Irvine, T. Lecuit, the Bloomington, Kyoto, DGRC and VDRC Drosophila reagent centers for antibodies and fly stocks. Thanks to Katy Ong, and other members of the DiNardo and Ghabrial labs and for comments on the work and

manuscript. We thank Andrea Stout and the CDB Microscopy Core for assistance and crucial advice on imaging. Supported by NIH R01 GM45747, GM60804.

References

Aldaz S, Escudero LM, Freeman M. Live imaging of Drosophila imaginal disc development. Proc Natl Acad Sci USA. 2010; 107(32):14217–14222. [PubMed: 20660765]

Aliee M, Roper JC, Landsberg KP, Pentzold C, Widmann TJ, Julicher F, Dahmann C. Physical mechanisms shaping the Drosophila dorsoventral compartment boundary. Curr Biol. 2012; 22(11): 967–976. [PubMed: 22560616]

Atwood SX, Prehoda KE. aPKC phosphorylates Miranda to polarize fate determinants during neuroblast asymmetric cell division. Curr Biol. 2009; 19(9):723–729. [PubMed: 19375318]

Bardet PL, Guirao B, Paoletti C, Serman F, Leopold V, Bosveld F, Goya Y, Mirouse V, Graner F, Bellaiche Y. PTEN controls junction lengthening and stability during cell rearrangement in epithelial tissue. Dev Cell. 2013; 25(5):534–546. [PubMed: 23707736]

Bertet C, Sulak L, Lecuit T. Myosin-dependent junction remodelling controls planar cell intercalation and axis elongation. Nature. 2004; 429(6992):667–671. [PubMed: 15190355]

Bertet C, Rauzi M, Lecuit T. Repression of Wasp by JAK/STAT signaling inhibits medial actomyosin network assembly and apical cell constriction in intercalating epithelial cells. Development. 2009; 136(24):4199–4212. [PubMed: 19934015]

Blankenship JT, Backovic ST, Sanny JS, Weitz O, Zallen JA. Multicellular rosette formation links planar cell polarity to tissue morphogenesis. Dev Cell. 2006; 11(4):459–470. [PubMed: 17011486]

Calzolari S, Terriente J, Pujades C. Cell segregation in the vertebrate hindbrain relies on actomyosin cables located at the interhombomeric boundaries. EMBO J. 2014; 33(7):686–701. [PubMed: 24569501]

Campbell G. Distalization of the Drosophila leg by graded EGF-receptor activity. Nature. 2002; 418(6899):781–785. [PubMed: 12181568]

Campbell G, Weaver T, Tomlinson A. Axis specification in the developing Drosophila appendage: the role of wingless, decapentaplegic, and the homeobox gene aristaless. Cell. 1993; 74(6):1113–1123. [PubMed: 8104704]

Casanova J, Sanchez-Herrero E, Morata G. Prothoracic transformation and functional structure of the Ultrabithorax gene of Drosophila. Cell. 1985; 42(2):663–669. [PubMed: 4028162]

de Celis Ibeas JM, Bray SJ. Bowl is required downstream of Notch for elaboration of distal limb patterning. Development. 2003; 130(24):5943–5952. [PubMed: 14573519]

Crossley PH, Martinez S, Martin GR. Midbrain development induced by FGF8 in the chick embryo. Nature. 1996; 380(6569):66–68. [PubMed: 8598907]

Currie DA, Milner MJ, Clive EW. The growth and differentiation in vitro of leg and wing imaginal disc cells from Drosophila melanogaster. Development. 1988; 102:805–814.

Dahmann C, Oates AC, Brand M. Boundary formation and maintenance in tissue development. Nat Rev Genet. 2011; 12(1):43–55. [PubMed: 21164524]

Farhadifar R, Roper JC, Aigouy B, Eaton S, Julicher F. The influence of cell mechanics, cell-cell interactions, and proliferation on epithelial packing. Curr Biol. 2007; 17(24):2095–2104. [PubMed: 18082406]

Fernandez-Gonzalez R, Zallen JA. Oscillatory behaviors and hierarchical assembly of contractile structures in intercalating cells. Phys Biol. 2011; 8(4):045005. [PubMed: 21750365]

Fernandez-Gonzalez R, Simoes Sde M, Roper JC, Eaton S, Zallen JA. Myosin II dynamics are regulated by tension in intercalating cells. Dev Cell. 2009; 17(5):736–743. [PubMed: 19879198]

Fraser S, Keynes R, Lumsden A. Segmentation in the chick embryo hindbrain is defined by cell lineage restrictions. Nature. 1990; 344(6265):431–435. [PubMed: 2320110]

Galindo MI, Bishop SA, Greig S, Couso JP. Leg patterning driven by proximal-distal interactions and EGFR signaling. Science. 2002; 297(5579):256–259. [PubMed: 12114628]

Garcia-Bellido A, Ripoll P, Morata AG. Developmental compartmentalization of the wing disc of Drosophila. Nat New Biol. 1973; 245:251–253. [PubMed: 4518369]

Hao I, Green RB, Dunaevsky O, Lengyel JA, Rauskolb C. The odd-skipped family of zinc finger genes promotes Drosophila leg segmentation. Dev Biol. 2003; 263(2):282–295. [PubMed: 14597202]

Hayashi T, Carthew RW. Surface mechanics mediate pattern formation in the developing retina. Nature. 2004; 431(7009):647–652. [PubMed: 15470418]

Kasza KE, Farrell DL, Zallen JA. Spatiotemporal control of epithelial remodeling by regulated myosin phosphorylation. Proc Natl Acad Sci USA. 2014; 111(32):11732–11737. [PubMed: 25071215]

Kojima T, Sato M, Saigo K. Formation and specification of distal leg segments in Drosophila by dual Bar homeobox genes, BarH1 and BarH2. Development. 2000; 127(4):769–778. [PubMed: 10648235]

Kojima T, Tsuji T, Saigo K. A concerted action of a paired-type homeobox gene, aristaless, and a homolog of Hox11/tlx homeobox gene, clawless, is essential for the distal tip development of the Drosophila leg. Dev Biol. 2005; 279(2):434–445. [PubMed: 15733670]

Landsberg KP, Farhadifar R, Ranft J, Umetsu D, Widmann TJ, Bittig T, Said A, Julicher F, Dahmann C. Increased cell bond tension governs cell sorting at the Drosophila anteroposterior compartment boundary. Curr Biol. 2009; 19(22):1950–1955. [PubMed: 19879142]

Langenberg T, Brand M. Lineage restriction maintains a stable organizer cell population at the zebrafish midbrain-hindbrain boundary. Development. 2005; 132(14):3209–3216. [PubMed: 15958515]

Lecuit T, Cohen SM. Proximal-distal axis formation in the Drosophila leg. Nature. 1997; 388(6638): 139–145. [PubMed: 9217152]

LeGoff L, Rouault H, Lecuit T. A global pattern of mechanical stress polarizes cell divisions and cell shape in the growing Drosophila wing disc. Development. 2013; 140(19):4051–4059. [PubMed: 24046320]

Major RJ, Irvine KD. Influence of Notch on dorsoventral compartmentalization and actin organization in the Drosophila wing. Development. 2005; 132(17):3823–3833. [PubMed: 16049109]

Major RJ, Irvine KD. Localization and requirement for Myosin II at the dorsal-ventral compartment boundary of the Drosophila wing. Dev Dyn. 2006; 235(11):3051–3058. [PubMed: 17013876]

Maroni G, Stamey SC. Use of blue food to select synchronous, late third instar larvae. Drosoph Inf Serv. 1983; 59:142–143.

Martin AC, Kaschube M, Wieschaus EF. Pulsed contractions of an actin-myosin network drive apical constriction. Nature. 2009; 457(7228):495–499. [PubMed: 19029882]

Mashburn DN, Lynch HE, Ma X, Hutson MS. Enabling user-guided segmentation and tracking of surface-labeled cells in time-lapse image sets of living tissues. Cytometry A. 2012; 81(5):409–418. [PubMed: 22411907]

Simões SM, Mainieri A, Zallen JA. Rho GTPase and Shroom direct planar polarized actomyosin contractility during convergent extension. J Cell Biol. 2014; 204(4):575–589. [PubMed: 24535826]

McMahon AP, Joyner AL, Bradley A, McMahon JA. The midbrain-hindbrain phenotype of Wnt-1-/Wnt-1- mice results from stepwise deletion of engrailed-expressing cells by 9.5 days postcoitum. Cell. 1992; 69:581–595. [PubMed: 1534034]

Mellitzer G, Xu Q, Wilkinson DG. Eph receptors and ephrins restrict cell intermingling and communication. Nature. 1999; 400(6739):77–81. [PubMed: 10403252]

Micchelli CA, Blair SS. Dorsoventral lineage restriction in wing imaginal discs requires Notch. Nature. 1999; 401(6752):473–476. [PubMed: 10519549]

Michel M, Aliee M, Rudolf K, Bialas L, Julicher F, Dahmann C. The selector gene apterous and notch are required to locally increase mechanical cell bond tension at the drosophila dorsoventral compartment boundary. PLoS One. 2016; 11(8):e0161668. [PubMed: 27552097]

Mitonaka T, Muramatsu Y, Sugiyama S, Mizuno T, Nishida Y. Essential roles of myosin phosphatase in the maintenance of epithelial cell integrity of Drosophila imaginal disc cells. Dev Biol. 2007; 309(1):78–86. [PubMed: 17662709]

Monier B, Pelissier-Monier A, Brand AH, Sanson B. An actomyosin-based barrier inhibits cell mixing at compartmental boundaries in Drosophila embryos. Nat Cell Biol. 2010; 12(1):60–65. [PubMed: 19966783]

Morata G, Lawrence P. The development of wingless a homeotic mutation of Drosophila. Dev Biol. 1977; 56:227–240. [PubMed: 849798]

Munjal A, Philippe JM, Munro E, Lecuit T. A self-organized biomechanical network drives shape changes during tissue morphogenesis. Nature. 2015; 524(7565):351–355. [PubMed: 26214737]

Nellen D, Burke R, Struhl G, Basler K. Direct and long-range action of a DPP morphogen gradient. Cell. 1996; 85(3):357–368. [PubMed: 8616891]

Oda H, Tsukita S. Real-time imaging of cell-cell adherens junctions reveals that Drosophila mesoderm invagination begins with two phases of apical constriction of cells. J Cell Sci. 2001; 114(Pt 3): 493–501. [PubMed: 11171319]

Price MH, Roberts DM, McCartney BM, Jezuit E, Peifer M. Cytoskeletal dynamics and cell signaling during planar polarity establishment in the Drosophila embryonic denticle. J Cell Sci. 2006; 119(Pt 3):403–415. [PubMed: 16418222]

Pueyo JI, Couso JP. Chip-mediated partnerships of the homeodomain proteins Bar and Aristaless with the LIM-HOM proteins Apterous and Lim1 regulate distal leg development. Development. 2004; 131(13):3107–3120. [PubMed: 15175252]

Pueyo JI, Galindo MI, Bishop SA, Couso JP. Proximal-distal leg development in Drosophila requires the apterous gene and the Lim1 homologue dlim1. Development. 2000; 127(24):5391–5402. [PubMed: 11076760]

Rauskolb C, Irvine KD. Notch-mediated segmentation and growth control of the Drosophila leg. Dev Biol. 1999; 210(2):339–350. [PubMed: 10357895]

Röper K. Supracellular actomyosin assemblies during development. Bioarchitecture. 2013; 3(2):45–49. [PubMed: 23760352]

Rudolf K, Umetsu D, Aliee M, Sui L, Julicher F, Dahmann C. A local difference in Hedgehog signal transduction increases mechanical cell bond tension and biases cell intercalations along the Drosophila anteroposterior compartment boundary. Development. 2015; 142(22):3845–3858. [PubMed: 26577205]

Sakurai KT, Kojima T, Aigaki T, Hayashi S. Differential control of cell affinity required for progression and refinement of cell boundary during Drosophila leg segmentation. Dev Biol. 2007; 309(1):126–136. [PubMed: 17655839]

Schneitz K, Spielmann P, Noll M. Molecular genetics of Aristaless, a prd-type homeo box gene involved in the morphogenesis of proximal and distal pattern elements in a subset of appendages in Drosophila. Genes Dev. 1993; 7(5):911. [PubMed: 8098308]

Simone RP, DiNardo S. Actomyosin contractility and Discs large contribute to junctional conversion in guiding cell alignment within the Drosophila embryonic epithelium. Development. 2010; 137(8): 1385–1394. [PubMed: 20332153]

Snodgrass, R. Principles of Insect Morphology. McGraw Hill; New York: 1935.

Tanimoto H, Itoh S, ten Dijke P, Tabata T. Hedgehog creates a gradient of DPP activity in Drosophila wing imaginal discs. Mol Cell. 2000; 5(1):59–71. [PubMed: 10678169]

Tsuji T, Sato A, Hiratani I, Taira M, Saigo K, Kojima T. Requirements of Lim1, a Drosophila LIM-homeobox gene, for normal leg and antennal development. Development. 2000; 127(20):4315–4323. [PubMed: 11003832]

Umetsu D, Aigouy B, Aliee M, Sui L, Eaton S, Julicher F, Dahmann C. Local increases in mechanical tension shape compartment boundaries by biasing cell intercalations. Curr Biol. 2014; 24(15): 1798–1805. [PubMed: 25065753]

Vasquez CG, Tworoger M, Martin AC. Dynamic myosin phosphorylation regulates contractile pulses and tissue integrity during epithelial morphogenesis. J Cell Biol. 2014; 206(3):435–450. [PubMed: 25092658]

Walters JW, Dilks SA, DiNardo S. Planar polarization of the denticle field in the Drosophila embryo: roles for Myosin II (zipper) and fringe. Dev Biol. 2006; 297(2):323–339. [PubMed: 16890930]

Winter CG, Wang B, Ballew A, Royou A, Karess R, Axelrod JD, Luo L. Drosophila Rho-associated kinase (Drok) links Frizzled-mediated planar cell polarity signaling to the actin cytoskeleton. Cell. 2001; 105(1):81–91. [PubMed: 11301004]

Wodarz A, Ramrath A, Kuchinke U, Knust E. Bazooka provides an apical cue for Inscuteable localization in Drosophila neuroblasts. Nature. 1999; 402(6761):544–547. [PubMed: 10591216]

Xu Q, Mellitzer G, Robinson V, Wilkinson DG. In vivo cell sorting in complementary segmental domains mediated by Eph receptors and ephrins. Nature. 1999; 399(6733):267–271. [PubMed: 10353250]

Zallen JA, Wieschaus E. Patterned gene expression directs bipolar planar polarity in Drosophila. Dev Cell. 2004; 6(3):343–355. [PubMed: 15030758]

Zartman J, Restrepo S, Basler K. A high-throughput template for optimizing Drosophila organ culture with response-surface methods. Development. 2013; 140(3):667–674. [PubMed: 23293298]

Zecca M, Basler K, Struhl G. Direct and long-range action of a wingless morphogen gradient. Cell. 1996; 87(5):833–844. [PubMed: 8945511]

Zervas M, Millet S, Ahn S, Joyner AL. Cell behaviors and genetic lineages of the mesencephalon and rhombomere 1. Neuron. 2004; 43(3):345–357. [PubMed: 15294143]

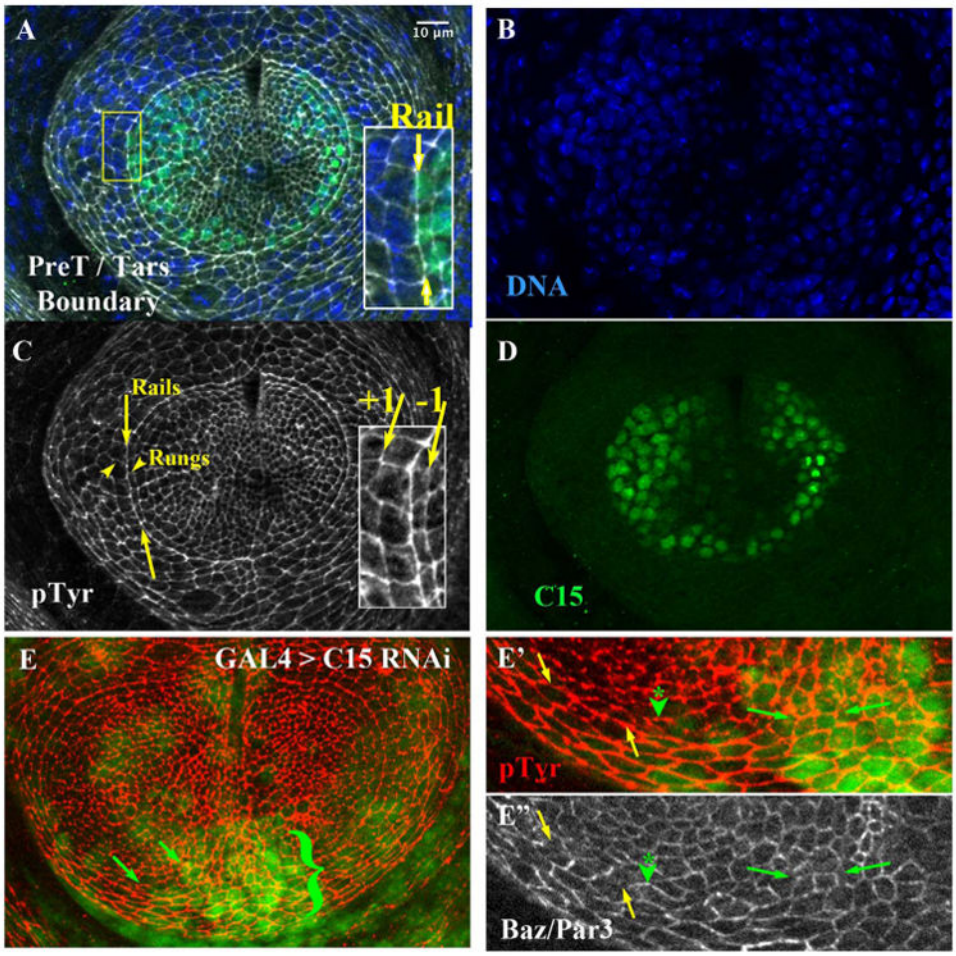

Fig. 1.

The pretarsal / tarsal aligned Arc Depends on C15. A) Late third instar leg disk triply labeled (merge in A) for B) DNA (Hoechst), C) Anti Phospho-Tyrosine (pTyr, white), and D) Anti-C15 (green). Inset in A: magnified view, where yellow arrows highlight the rail interface comprising the tarsal / pretarsal boundary. C) The area between the yellow arrows highlight a portion of rail interfaces; arrowheads highlight two rungs, located orthogonal to rail interfaces. The inset highlights interfaces made from cells one cell column to the inside of the rail (−1 interface) or one column to the outside (+1 interface). E) A small clone of cells expressing C15 RNAi, marked by nuclear GFP. Cell outlines revealed by pTyr (Red). The area adjacent to the bracket exhibited a disruption in smoothness of the rail. E′ and E″) Magnification of the lower portion of the arc. The yellow arrows first highlight a section of the rail not subject to C15 RNAi. This wild-type portion of the rail was relatively depleted for Bazooka/Par3 (E″, white, section between yellow arrows), while orthogonal rungs were enriched as expected (see forward to Fig. 2C′ and D). In contrast, in cells or regions affected by C15 RNAi (at the green arrowhead, and the section between the small green arrows) Bazooka/Par3 accumulated ectopically on horizontal interfaces, rather than being restricted to orthogonal boundaries. Scale bar applied to insets of A, C, or panel E′, E″ would be 5 μm.

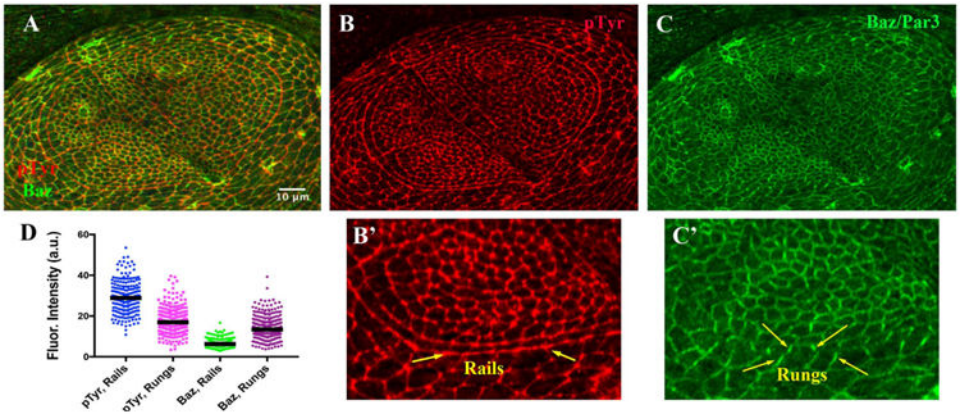

Fig. 2.

Relative Enrichments of pTyr along Rails & Baz along Rungs. A – C). Late third instar leg disk doubly labeled, merge in A, for B) Anti Phospho-Tyrosine (pTyr, Red), and C) Anti-Bazooka (Green). B′ and C′) Magnification of the lower portion of the arc, within the Posterior compartment. The area between the yellow arrows highlight the rail, enriched for pTyr, and relatively depleted for Baz, which instead was enriched on rungs, located orthogonal to rail interfaces. D) Scatter plot for fluorescence intensities (in arbitrary units), with bar representing the median value. Scale bar applied to B′, C′ would represent 5 µm.

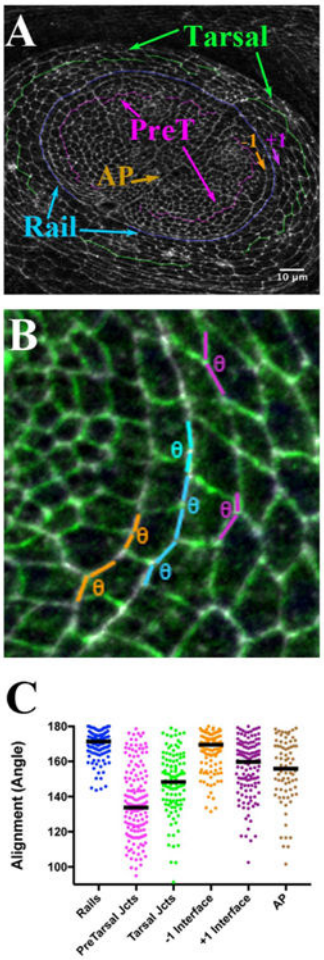

Fig. 3.

The Rail is more aligned than surrounding interfaces, including the AP boundary. A) Late third instar leg disk labeled for Anti Phospho-Tyrosine (White). Rail interfaces are highlighted in blue, while interfaces flanking the rail are indicated as inner, −1 in orange, and outer, +1 in purple. Example interfaces away form the rail boundary and well within the pretarsal and tarsal regions are also highlighted: pretarsal in magenta, and tarsal in green. Finally, the AP compartment boundary is indicated (brown Arrow). B) The scheme for measuring alignment is shown. Angles were scored along rail, the −1 (orange), and the +1 (purple) interfaces, as well as along interfaces further inside the pretarsal and tarsal regions, and along the AP compartment boundary. Overall the rail gently curves. However, adjacent interfaces that make up the rail approach each other in rather straight fashion, forming adjoining line sections. The maximum angle between a pair of joined straight lines is 180°. Thus, to compare relative alignment between the rail and other interfaces within the epithelium, we measured the angles at which each pair of rail interfaces meets. For example, six sections, representing consecutive rail interfaces, are highlighted in blue. The angle formed by each pair was measured with the angle tool in Image J (θ symbol). The more aligned each pair of sections, the closer to 180° the angle. Obviously, two of the highlighted examples approach 180°, while, for a more wiggly interface, the angle will be less, approaching 120°. While, in principle, a wiggly interface can form at greater than a 180°

angle (a reflex angle), for simplicity, we set Image J to return (360° – reflex angle value). C) Scatter plot of alignment angles (in degrees), with bar representing the median value. Scale bar applied to B would be 3 μm.

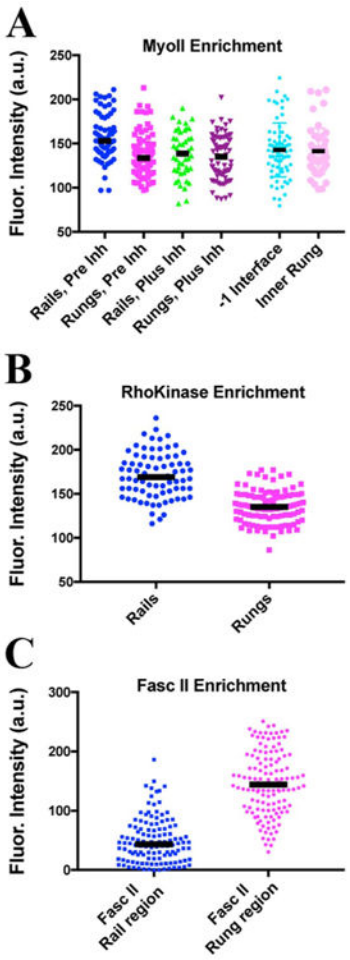

Fig. 4.

Myosin II and Rho Kinase are enriched on Rails, while Fasciclin II is enriched on orthogonal interfaces. Scatter plot for fluorescence intensities (in arbitrary units), with bar representing the median value. Data in A and B are from live imaging. A) Regulatory light chain::mCherrry (Sqh::mCherry) values for rail (blue dots, Pre Inh) and rungs (magenta dots, Pre Inh) before treatment of disks with a Rho Kinase inhibitor. An example RLC::mCherry disk is shown in Fig. 6A″. The same disks about 40 min after treatment with the Rho Kinase inhibitor: rail (green dots, Plus Inh) and rungs (purple dots, Plus Inh). An example RLC::mCherry disk after Rho K treatment is shown in Fig. 6B″. Since we noted significant alignment of the interfaces flanking the rail, we considered whether RLC-mCherry might be enriched on these flanking interfaces (before inhibitor treatment). However, there was no obvious enrichment, and quantitation confirmed observed no significant difference in RLC-mCherry comparing the −1 interface and the adjacent inner rung interfaces (light blue and light magenta dots; median fluorescence was 132 versus 146, $p = 0.52$; 4 disks, 52 and 74 interfaces, respectively). B) Rho Kinase::GFP levels (RhoK{K116A} (Simões et al., 2014)) comparing rail interfaces (blue dots) and rung interfaces (magenta dots). C) Quantitation of Fasciclin II levels in fixed and stained disks. Since Fasc II accumulates just basal to the adherens junction (as defined by the domain of highest pTyr signal), Fasc II was quantified from the region just beneath the rail (blue dots) and just below the rung (magenta dots).

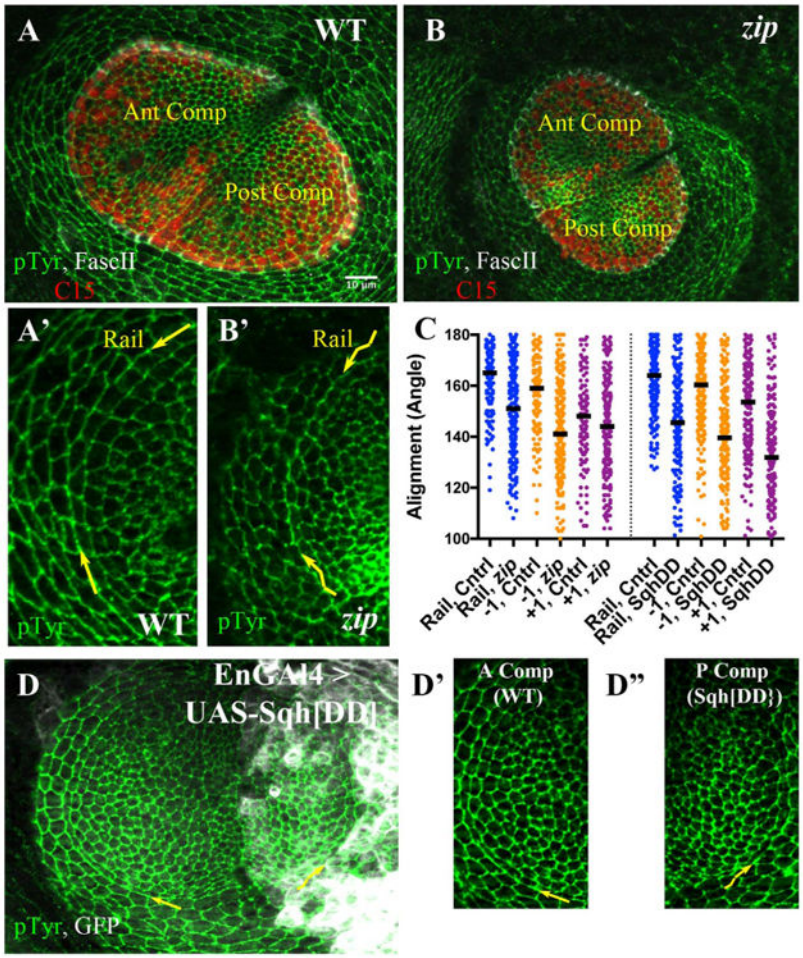

Fig. 5.

Alignment requires Myosin II function. A, B) Late third instar leg disks labeled with anti-PTyr (green), C15 (red) and Fasc II (white). A) Sibling control; anterior and posterior compartments are indicated. A′) A sector of the A compartment including rail is shown at increased magnification (pTyr channel only). The curving rail interface is highlighted by yellow arrows. B) zip mutant disk. B′) A sector of the A compartment including rail is shown at increased magnification (pTyr channel only). The wiggly appearance of the rail interface is obvious, and highlighted by wiggly yellow arrows. C) Scatter plot of alignment angles (in degrees), with bar representing the median value. The left half presents angles measurements for control (heterozygous siblings) versus *zip2/zipEbr* mutants, for the rail (blue), the −1 (orange) and the +1 (purple) interfaces. The right half of the scatterplot presents angle measurements for control (anterior compartment) versus cells expressing Sqh. DD (posterior compartment), for the rail (blue), the −1 (orange) and the +1 (purple) interfaces. **D**) Representative disk from En-GAL4 > UASGFP, UAS-Sqh. DD larva, stained for pTyr (green) and GFP (white). The yellow arrows draw attention to the rail interfaces within the anterior or posterior compartment, which are featured at higher magnification in D′, D″. D′) Control cells (anterior compartment), arrow points along rail interface. D″) Cells expressing Sqh. DD (posterior compartment), wiggly arrow points along rail interface. Scale bar applied to A′, B′, D′, D″ would be 5 μm.

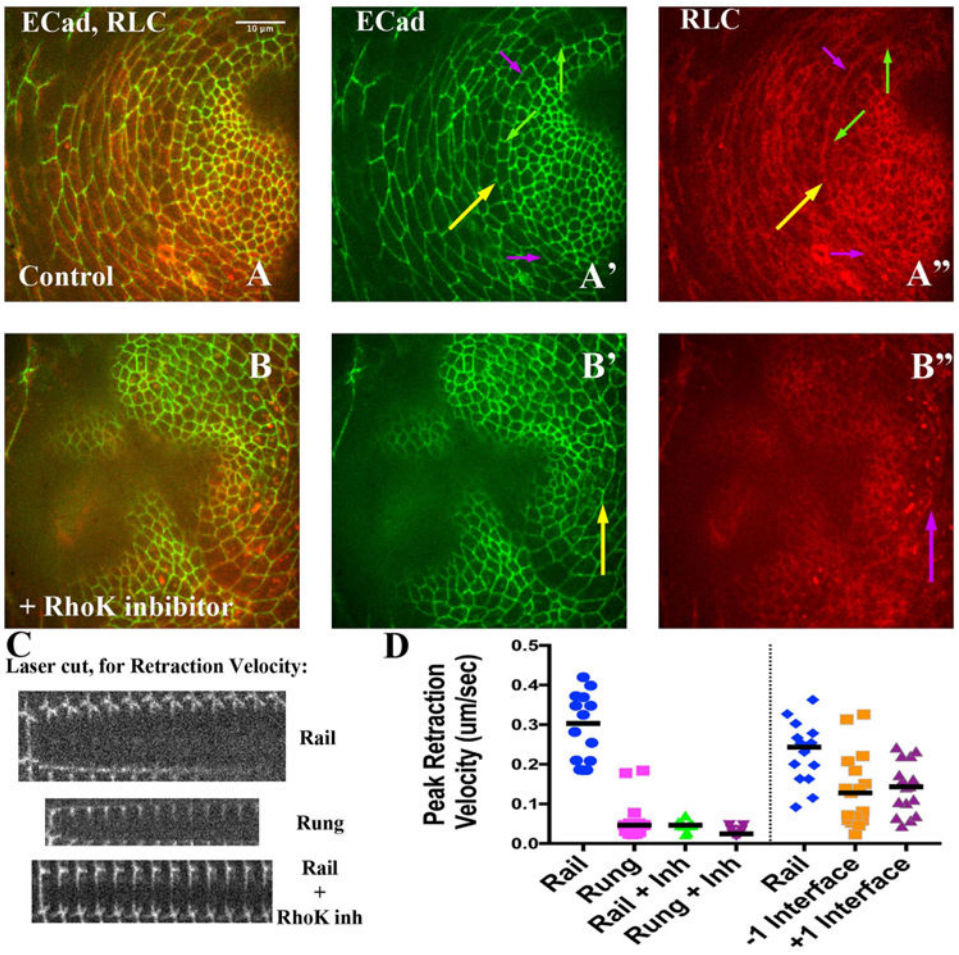

Fig. 6.

Tension along Rails is significantly decreased by Rho Kinase inhibitor treatment. A and B) Late third instar disks imaged live, expressing ECadeherin::GFP (A′, B′, green) and RLC::mCherry (A″ and B″, red). Yellow arrows highlight the rail. A′) The purple arrows point out example rail interfaces that would have been targeted for ablation while green arrows point out rung interfaces (see panel C, below). A″) Note relative enrichment of RLC::mCherry along rails (purple arrows) compared to rungs (green arrows). B – B″) A different disk, about 30 min after treatment with the Rho Kinase inhibitor. B′) Yellow arrows point to a rail interface. B″) Note how area of rail interface has lost RLC::MCherry enrichment; and instead exhibits more punctate signal. C) Three montages, from top to bottom representing three example laser ablations: a rail, a rung, and a rail interface after addition of the Rho Kinase inhibitor. In each, the first strip of the montage is before ablation, while subsequent strips are at 5-s intervals (see Section 4). D) Normalized peak reaction velocity is presented in a scatter plot. Scale bar applied to montages would be 5 μm.

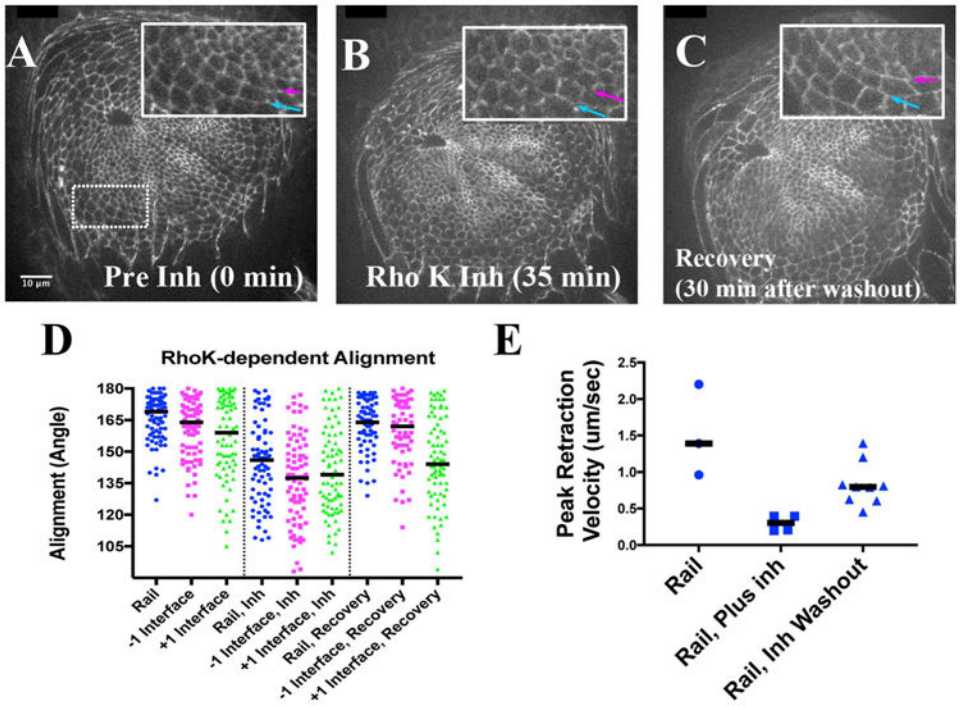

Fig. 7.

Relative Rail Alignment depends on Rho Kinase. A-C) Stills from a live imaging session. A) Before the addition of Rho Kinase inhibitor. Inset: magnified view of boxed area. Blue arrow highlights the rail, while the magenta arrow highlights the −1 interface. B) About 35 min after addition of Rho Kinase inhibitor (see Section 4.4). The blue and magenta arrows point to the same interfaces as in panel A. C) About 30 min after wash-out of the inhibitor (~150 min relative to panel A). D) Scatter plot of alignment angles (in degrees) of rail, −1 and +1 interfaces, with a bar marking the medians. The left-hand section of plot is before addition of Rho Kinase inhibitor, the middle represents alignment in the presence of the inhibitor, and the right-hand side represents alignment after recovery (after wash-out of inhibitor). E) Scatter plot representing normalized peak reaction velocities for rail interfaces before, during and after recovery from Rho Kinase inhibitor treatments. Scale bar applied to insets would be 6 μm.